SAND2014-1023C
Proceedings of the ASME 2014 Pressure Vessels & Piping Division Conference
PVP2014
July 20-24, 2014, Anaheim, California, USA

PVP2014-28336

AN EXPERIMENTAL STUDY OF DUCTILE FAILURE UNDER MULTI-AXIAL LOADING

Wei-Yang Lu
Sandia National Laboratories
Livermore, CA, USA

Helena Jin
Sandia National Laboratories
Livermore, CA, USA

ABSTRACT

Recent experimental investigations show that most models are not able to capture the ductile behavior of metal alloys in the entire triaxiality range, especially at low triaxiality. Modelers are moving beyond stress triaxiality as the dominant indicator of material failure and developing constitutive models that incorporate shear into the evolution of the failure model. Available data that cover low triaxiality range are rare and a series of critical experiments is needed. Here, experiments of smooth thin as well as notched tubular specimens of Al6061-T651 under combined tension-torsion loading were conducted. This provides a very basic set of data for phenomenological models. A full-field deformation technique, digital image correlation (DIC), was applied to these tests to allow measurement of the field deformation, including the notched area. The microstructural features of the tested specimens were characterized to better understand the different failure mechanisms which led to ductility variation in the aluminum alloy.

INTRODUCTION

Ductile failure of metals remains an active research field although it has been through a long history of investigation. Significant progresses have been made in characterizing, understanding, and predicting the phenomenon. Experiments of carefully designed specimens had been conducted, such as cylinders with notched geometry for tension, uniform tubular specimen for torsion, etc. Johnson-Cook fracture model [1], for example, was developed based on the experimental stress and strain data. The strain at fracture $\bar{\varepsilon}_f$ is described by

$$\bar{\varepsilon}_f = C_1 + C_2 \exp(C_3\eta) \quad (1)$$

where C1, C2 and C3 are constants and the stress triaxiality η is a ratio of the mean stress σ_m to the equivalent stress $\bar{\sigma}$. A similar result was also obtained from micromechanics modeling approach based on the microstructure aspect of ductile fracture. Void nucleation, void growth and void coalescence are strongly dependent on stress triaxiality [2].

A relatively recent experimental study of 2024-T351 aluminum alloy by Bao and Wierzbicki [3] included a series of tests with specimens of various geometries and loadings to cover a wide range of triaxiality. The results demonstrate that there need three distinct functions of $\bar{\varepsilon}_f(\eta)$ to fit the experimental data instead of one. As shown in Fig. 1, there is a local maximum at $\eta = 0.4$. The triaxiality axis are divided into three ranges I, II, and III, corresponding to high, low, and negative stress triaxialities; each has its own function to represent the failure strain. A typical classical damage model has only one smooth curve for all positive triaxialities. The data show a different trend from model in the low triaxiality range, i.e. shear dominated loading, where classical model overestimates failure strain. This discrepancy has motivated many new studies to focus on the failure behavior in Range II. Other parameter, such as Lode parameter, that may have effect ductile failure has been suggested.

The available data for the share dominated experiments are very limited. In this paper, the plasticity and failure behavior of Al6061-T651 is investigated. The study is limited to positive triaxialities and particular attention is paid to the experimental aspects of shear dominated loadings. A brief review of new published experiments is presented followed by reporting a series of tension-torsion test of tubular specimens.

Copyright © 20xx by ASME

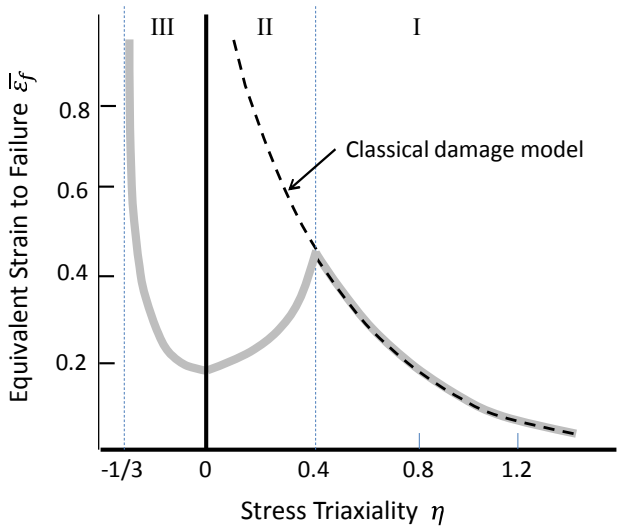

Figure 1 Equivalent strain at failure of Al2024-T351. Solid lines are curves fit to experimental data (from [3]).

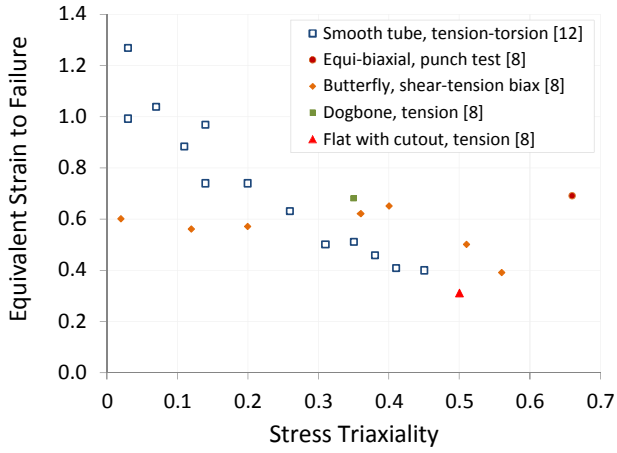

Figure 2 Failure strain of Al6061-T6. (Data from [8] and [12].)

REVIEW OF RECENT EXPERIMENTS

Following the work of Bao and Wierzbicki [3], a number of experimental studies on ductile failure [4-13] have been published. They are listed in Table 1, where the materials of interest, methods to determine the failure strain, and types of tests performed are summarized. Wierzbicki and his co-workers [4, 6-7] extended their investigations to different aluminum alloys and steels. Other researchers were also interested in similar materials.

A majority of studies used the hybrid experiment-simulation method to determine the equivalent strain at failure. That is, the location of incipient failure was determined from experimental observation, but the equivalent strain and stress triaxiality were obtained from the simulation that matched the load-displacement response and at the failure location [3]. Unfortunately, for in-plane shear cases the initial failure location could not be clearly identified experimentally according to the authors, and the point in the center of the deformation zone was chosen to represent the strain behavior [3, 8].

Among various experiments, high triaxiality failure experiments typically include smooth and notched round bar or plate dog-bone and grooved plate tension, which are standard and widely accepted. The experiments for low triaxiality, however, were evolving. Variations of specimen geometry and loading configurations were reported. In general, it could be divided into two categories: butterfly [3, 4, 7-8, 11] and tubular [5, 6, 10, 12-13] specimens. There were four different butterfly geometries considered in these studies: (1) plate butterfly [3, 8, 11], (2) plate butterfly with a notch [8], (3) modified butterfly II with double curvature at the gage section [4], and (4) modified butterfly III. The first three were subjected to in-plane tensile loading in various angles and the fourth one was for tension-shear biaxial loading. The tubular specimen was either smooth [6, 10, 12] or double notched [5, 10, 13] tube.

For negative triaxiality experiments, cylinder, notched cylinder [3], and shear compression disk [9] were used. Since the focus of this paper is on the low triaxiality, Range II on Fig. 1, the experiments deal with Range III will not be discussed here.

Most studies support the conclusion by Bao and Wierzbicki [3] that there is a local maximum and possible slope discontinuity in the fracture locus in the $\bar{\varepsilon}_f - \eta$ plot [4-7, 13]. On the other hand, there are some studies show that the local maximum phenomenon is not clear, and the failure strain increases monotonically as the stress triaxiality decreases [6, 8, 12]. With many materials as well as various experimental and measuring methods involved, conclusions are different. Material is certainly a factor. In the work of Bai et al. [6], two different steels were tested and measured under the exact same condition, but showed different results. Is there something else? Aluminum alloy 6061-T6 was involved in multiple investigations and the results of failure strain and triaxiality of Al6061-T6 are provided numerically [7, 12], which are plotted in Fig. 2. These two sets of data show quite different trends. The discrepancy must come from the experimental and measuring methods.

It is quite obvious that, for various types of samples and under controlled loading conditions, researchers have tried to measure the same quantities: the stress and strain at the location when and where the failure initiates. It is a very challenging work and approximations and assumptions are inevitable. The experiment and specimen affect how failure stress and strain are determined and its accuracy; the method of obtaining local failure strain is a common issue. More detail discussion of recent low triaxiality experiments and the methods to determine failure strain are in the following.

Copyright © 20xx by ASME

Table 1 Triaxial Experiments

Experiment	1st Author Year Ref		Bao 2004 [3]	Wierzbicki 2005b [4]	Barsoum 2007 [5]	Bai 2009 [6]	Beese 2010 [7]	Gruben 2011 [8]	Dorogoy 2011 [9]	Lu 2012 [10]	A.G. 2013 [11]	H
Material			Al2024 -T351	A710 steel	Weldox 420 & 960 Steel	1045 steel DH36	Al6061 -T6	Docol 600DLs teel	4340 steel & Al7075-	Al6061 -T651	Al6061 -T6	A
Measurement Method			Numerical Simulation (NS)	NS	NS	NS	DIC, NS, Area Reduction	DIC, NS	NS	DIC	DIC, Grain Analy.	
Specimen Type	**T**	**L**										
Smooth round bars, tension	H	1	x			x				x		
Plate dogbone	H	0 - 1	x				x	x				
Plate plane strain, tension	H	0	x				x	x				
Flat specimen with cut out	H	0 - 1	x				x					
Smooth tube, tension	H	0								x		
Notched round bars, tension	H	1	x			x				x		
Flat grooved plates, tension	H	0	x			x	x					
Punch test on circular disk	H	-1					x					
Butterfly I (in-plan shear), tension	L	0	x					x			x	
Notched Arcan	H, L	0 - 1						x				
Butterfly II, tension or compression	H, L, N	-0.5 - 1		x								
Butterfly III, tension & shear	H, L	0 - 1					x					
Smooth tube, torsion	L	0				x				x		
Smooth tube, tension/torsion	H, L	-										
Double notched tube, tension and torsion	H, L	0 - 1			x					x		
Shear Compression Disk	L, N	-							x			

Copyright © 20xx by ASME

Recent Low triaxiality experiment

The plate butterfly type specimen has been widely utilized to characterize the shear properties of composite materials [14-15] and metals. The shear stress distribution is nearly constant for most part of the gage section, but toward the surface boundaries the stresses are very different; therefore, the triaxialities at the boundary and at the center of the shear deformation zone are not the same. Evidences that the failure initiated at the boundary were reported [4, 11]. In some tests the initial failure location of such specimen could not be clearly identified experimentally [3, 8] and assumed the failure initiated at the center. The assumption may be not valid. If the initial failure was happened at the edge, then the failure could actually belongs to the high triaxiality range even most of the section was loaded under low triaxiality.

The new design of modified butterfly II or III eliminates the problem of initial failure location and ensures that strain is highly localized in the central gage section. The geometry of these specimens is more complex. The stress distribution is very non-uniform in the gage section and evaluating stress accurately becomes challenging [12].

The other kind of shear specimen is the tubular geometry, which has been commonly used to obtain multi-axial material properties in metal plasticity. The axisymmetric feature of geometry, stress and strain distributions, etc. makes data analysis more efficient and accurate. Determine the failure stress at failure is less complex. Double notched tube specimen potentially has several advantages over smooth tube. It can have a wider range in triaxiality, avoid buckling of a thin walled cylinder under shear, and confine the onset of fracture processes to the notch region [13].

Methods of Failure strain Measurement

To accurately determine the local strain at failure is quite difficult. In addition to commonly used experimental-numerical hybrid method, experimental methods such as digital image correlation (DIC), grid method, area reduction, and microstructural grain analysis have been applied. The hybrid method utilizing finite element simulation is heavily dependent on the validity of the constitutive equation of the material, which must be accurate in all possible multi-axial and large deformations. A detail discussion about the requirement of a constitution equation in hybrid method is given in [12]. Without a validated constitutive equation, the method does not provide an accurate measurement and the uncertainty is unknown. Comparing to other experimental method at the same failure location, strains determined from numerical simulation, area reduction and DIC often give different values in one study [7].

Grid method and microstructural analysis [11-12] produce consistent measures of strain at failure. The results show the localized strain is concentrated in a very narrow zone and the shear strain could reach a very large value, more than 1.2.

EXPERIMENTS

In this work, a series of experiments were conducted for the purpose of characterizing the plasticity and failure behavior of Al6061-T651 and calibrating model parameters [10]. A number of tests were included as listed in Table 1. All specimens were machined from a certified Al6061-T651 solid bar with a diameter of 38.1 mm (1.5 inch). From microstructural analysis, the average grain size is about 200 μm. Smooth tensile specimens were obtained from axial and transverse directions of the aluminum bar. The gage section had a diameter of 2.54 mm (0.1 inch). Notched tensile specimens had three different notch radiuses: 1.0, 2.0 and 10.0 mm. They all had the same minimum and maximum diameters, 6.35 and 12.7 mm (0.25 and 0.5 inch), respectively. For smooth tubular specimens, the inside and outside diameters at the gage section were 18.03 and 19.05 mm (0.71 and 0.75 inch). The gage length was 12.7 mm (0.5 inch). Double notched tubular specimen had only one notch radius of 3.175 mm (0.125 inch). At the root of the notch, the wall thickness was 508 μm (0.02 inch) and the center of the thickness was located at the circle with a diameter of 22.23 mm (0.875 inch). The tube had the inside and outside diameters of 19.05 and 24.5 mm (0.75 and 1.0 inch), respectively. The axes of notched tensile specimens and all tubular specimens were along the same direction of the bar material.

Most tests were conducted on an axial-torsional biaxial tabletop testing system, which has the capacity of 13 kN and 16 N-m (3,000 lb and 1,500 in-lb). Notch tensile tests were performed on a different axial system with 100 kN capacity. Figure 3 and 4 show the setups of tensile and biaxial experiments, respectively. An extensometer was used to measure the extension of tensile specimens; the deformation of tubular specimens was evaluated by using 3D DIC method.

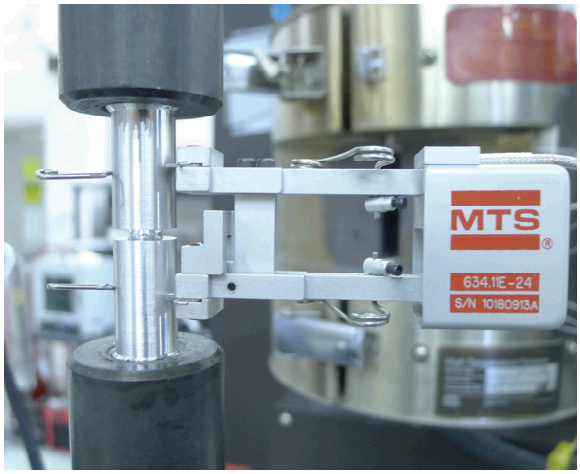

Figure 3 Tensile experiment setup.

Copyright © 20xx by ASME

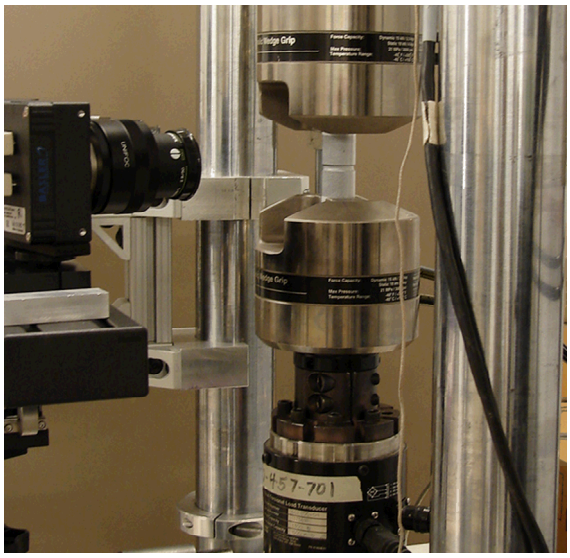

Figure 4 Setup for biaxial experiments.

Tests were conducted under actuator displacement and rotation control. The loading was quasi-static. Load, torque, displacement, rotation, and extensometer output or DIC images were recorded.

RESULTS AND DISCUSSION

Smooth round bar tension

Among several repeats of tensile tests, two typical engineering stress-strain curves of the material, one in the axial direction and the other in the transverse direction, are plotted in Fig. 5. The axial direction has a slightly lower yield stress but much longer elongation, 0.21 versus 0.15. This indicates that the plastic behavior of the material is nearly isotropic, but damage evolution appears to be anisotropic. The pictures of corresponding failed specimens are shown below the break point of the curve. The failure surface of the axial specimen exhibits a cup and cone geometry, while the transverse specimen displays an angled surface like shear failure. The anisotropic failure is similar to that has observed on a cold rolled material Al7075-T351 [16]. In an in-situ X-ray tomography experiment, it shows the void growth mechanisms are different in three principal material axes. Anisotropic failure was considered by Beese, et al. [7], but was generally neglected.

Notched round bar tension

Figure 6 shows the load-displacement curves of the notched specimen tension. Each case had three repeats. The result is very consistent and only one curve for each case is plotted. The displacement is the extension of the gage section measured by an extensometer. The gage section is 25.4 mm (1.0 inch) in distance with the notch at the center.

Thin smooth tubular specimen

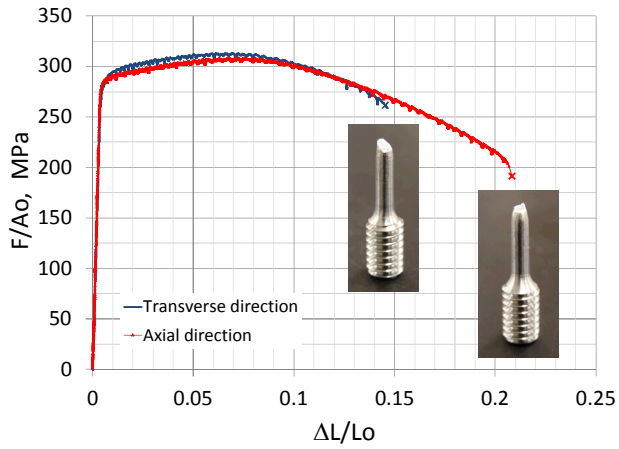

Figure 5 Tensile engineering stress-strain curves.

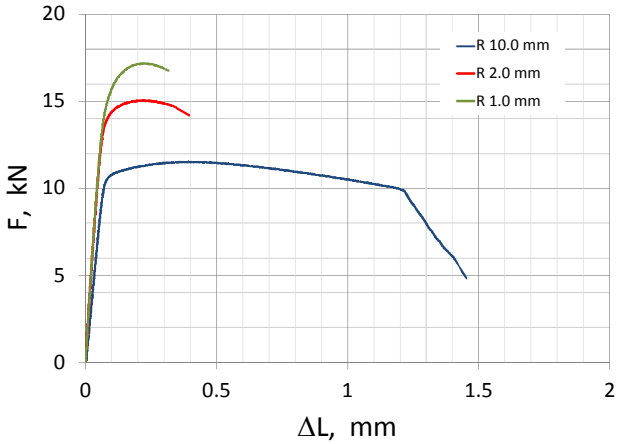

Figure 6 Load-displacement curves of notched specimen tension.

Two loading paths were applied successfully for thin smooth tube tests: tensile, Specimen F01, and combined tension torsion, Specimen F03. The results are plotted in Fig. 7. Although the controlled displacement-rotation path for F03 was linear, the strain path was slightly curved and the stress path was clearly non-proportional after yield. The averaged strains are calculated from the data in the area of interest, which is typically the overlap between the DIC measurable area and the gage section of the specimen. The images for DIC analysis were recorded at one frame per second. Figure 8(a) shows the major strain distribution of F01, which was analyzed from the last frame of images before failure, at t = 259 s; Figure 8(b) shows the next frame at t = 260 s, where the specimen is separated in two. At t = 259 s, the averaged major strain is about 0.085, but reaches approximately 0.18 at the location leading to failure. Shown in Fig. 9, the deformation of F03 was generally uniform until close to failure. A localized band appeared just before the specimen broke. Thin wall buckling was not detected.

Copyright © 20xx by ASME

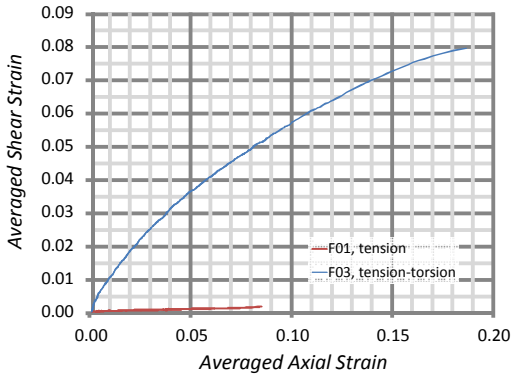

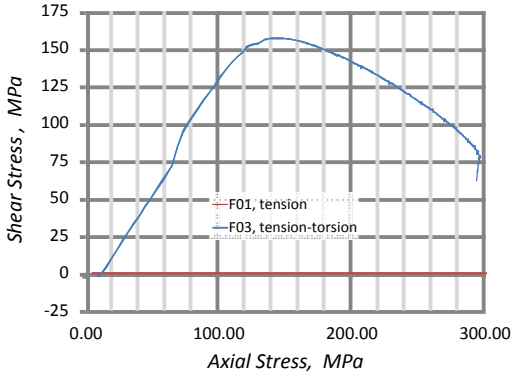

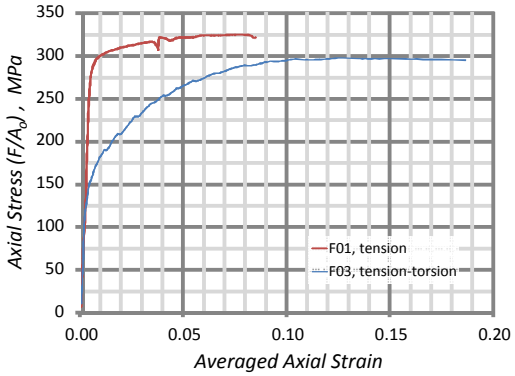

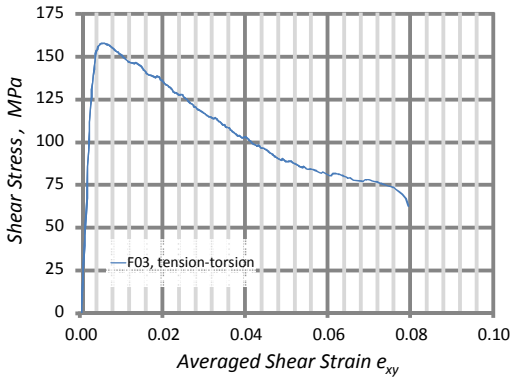

Figure 7 Results of smooth tube experiments.

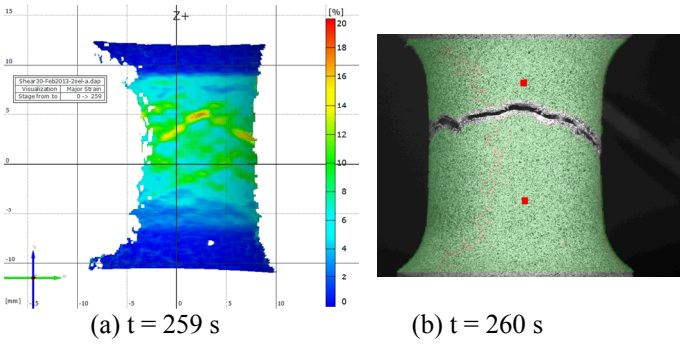

Figure 8 (a) The major strain distribution of F01 before failure; (b) the left image of specimen after failure.

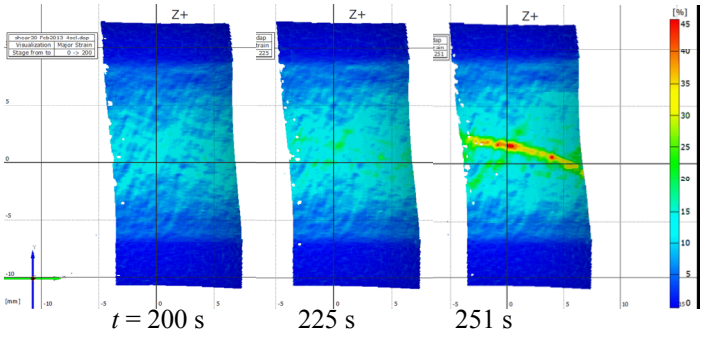

Figure 9 Deformation history of smooth tube F03.

Double noticed tubular specimen

The deformation of the notched tube was measured by using 3D DIC method. Figure 10(a) shows displacement Δy (= $y - y_o$) versus original position y_o curves at different stages of tensile loading of Tube04 specimen. There are numbers of curves in the plot defined by the stage number, which specifies the image frame taken sequentially during loading. The stage number increases as the displacement becomes larger and the curve shifts right. For #433, which is the last image before failure, the corresponding surface plot is also displayed with the matching y-axis scale. Similarly, Fig. 10(b) shows the axial strain e_{yy}. Above and below the notch area, the Δy curves are linear and the deformation is elastic. Clearly, the plastic deformation is concentrated in a narrow band at the root of the notch.

The deformation paths and corresponding load-torque paths as well as load-displacement and torque-angle curves of a series of tests (two tension, two torsion and two combined tension-torsion tests) are plotted in Fig. 11. Since the actuator displacement includes system compliance and maybe specimen slip in the grips, the displacement of the specimen defined here covers only the center 16 mm of the specimen. That is 8 mm above and8 mm below the root of the notch as shown in Fig. 10(a). The value is calculated from the DIC result. Similarly, the angle of rotation $\Delta\theta$ of the specimen is obtained the same way.

Copyright © 20xx by ASME

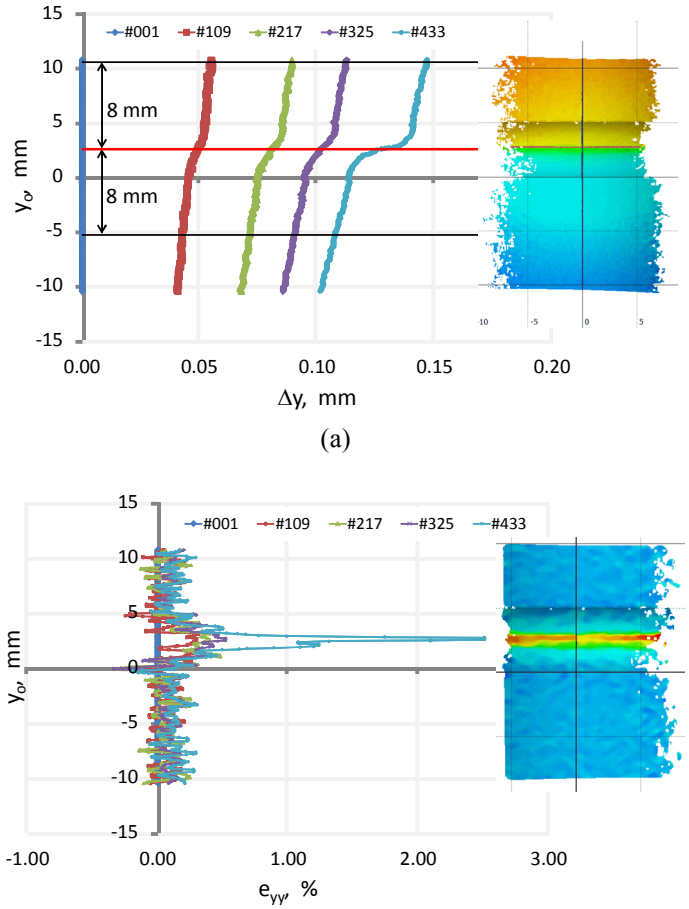

Figure 10 Tube04 displacement and strain fields at different stages of loading.

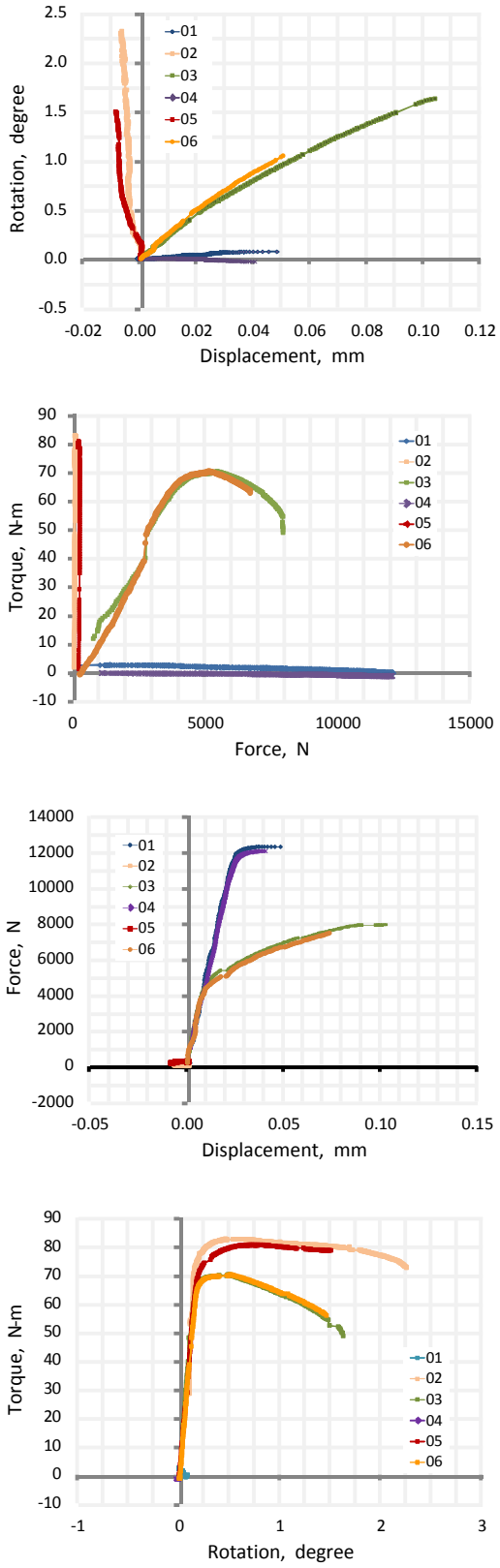

Figure 11 Results of notched tube experiments.

The values of Δy and Δθ are accurate since the speckle pattern and the deformation at the location of evaluation is well behaved, smooth, continuous and moderate displacement. At the root of the notch, especially at large rotation, both strain and strain gradient are high. As reported in [11], the width of the narrow deformation band is about 200 - 500 μm for Al6061-T6. Considering the speckle pattern used, the uncertainty of shear strain measurement could also be large at large strain. That makes localized failure strain characterization very challenging. In one of the torsion test Tube05, the speckle pattern at that highly deformed area became not workable at stage #236; the specimen failed at stage #301. The measurement could be improved by using finer speckle patterns and higher resolution camera.

There is another issue about using 3D DIC to characterize localized shear failure strain. Even the measurement covers a large area, but it is still only includes a fraction of the whole surface and may miss the initial failure location. Like torsion test Tube02, the maximum shear strain from DIC was $e_{xy} = 0.37$

Copyright © 20xx by ASME

but failure was not occurred in the measured area. Further study, microstructural analysis for example, is needed to characterize the failure strain of these tests.

The fractographs of three different loadings are shown in Fig. 12. The fracture surface, shown in Fig. 12(a), exhibits deep dimples, typical for ductile tensile failure. Figure 12(c) shows shear failure, which has shallow grooved surface along the shear direction. The combined tension-torsion specimen shows a mix of two modes, Fig. 12(b). Steels have the similar result [5].

CONCLUSIONS

The influence of triaxiality and Lode parameter on ductility has been the focus of recently published experiments on ductile failure. Many different tests, measurement and analysis techniques have been reported to determine the local stress and strain at the incipient of failure. Results are not consistent. It appears that the experimental trend is: more physical measurement methods are involved lately then the numerical simulation hybrid method; also, more tension-torsion tubular specimens than butterfly types of specimens.

A series of experiments for model calibration and characterization of Al6061-T651 as well as for study its ductile failure behavior is reported in the paper. The 3D DIC method was applied to measure the deformation field. The results on failure characterization are qualitative and not complete. Future study and improvement are needed to do it quantitatively.

ACKNOWLEDGMENTS

Sandia is a multiprogram laboratory operated by Sandia Corporation, a Lockheed Martin Company, for the United States Department of Energy under contract DE-AC04-94-AL85000.

REFERENCES

[1] Johnson, G.R., and Cook, W. H., 1985, "Fracture Characteristics of Three Metals Subjected to Various Strains, Strain Rates, Temperatures and Pressures," Eng. Fracture Mechanics, 21(1), pp.31-48.

[2] Garrison Jr., W.M., and Moody, N.R., 1987, "Ductile Failure," J. Phys. Chem. Solids, 48, pp. 1035-1074.

[3] Bao, Y., and Wierzbicki, T., 2004, "On Fracture Locus in the Equivalent Strain and Stress Triaxiality Space," Int. J. Mech. Sci., 46(1), pp. 81–98.

[4] Wierzbicki, T., Bao, Y., and and Bai, Y., 2005, "A New Experimental Technique for Constructing a Fracture Envelope of Metals under Multi-axial loading," Proceedings of the 2005 SEM annual conference and exposition on experimental and applied mechanics. pp. 1295–1303.

[5] Barsoum, I., and Faleskog, J., 2007, "Rupture mechanisms in combined tension and shear—Experiments," Int. J. of Solids and Structures, 44, pp. 1768–1786.

[6] Bai, Y., Teng, X., and Wierzbicki, T., 2009, "On the Application of Stress Triaxiality Formula for Plane Strain Fracture Testing," J. Eng. Mat. Tech., 131(2), Article #021002.

[7] Beese, A. M., Luo, M., Li, Y., Bai, Y., and Wierzbicki, T., 2010, "Partially coupled anisotropic fracture model for aluminum sheets," Eng. Fracture Mechanics 77, pp. 1128–1152.

[8] Gruben, G., Fagerholt, E., Hopperstad, O.S., and Børvik, T., 2011, "Fracture characteristics of a cold-rolled dual-phase steel," European J. of Mechanics A/Solids, 30, pp. 204-218.

[9] Dorogoy, A.,Karp, B., and Rittel, D., 2011, "A Shear Compression Disk Specimen with Controlled Stress Triaxiality under Quasi-Static Loading," Experimental Mechanics, 51, pp. 1545–1557.

[10] Lu, W.-Y., and Jin, H., 2012, "Ductility of Al Alloys under Various States of Stress Triaxiality," IMECE2012.

[11] Ghahremaninezhad, A., and Ravi-Chandar, K., 2013, "Ductile failure behavior of polycrystalline Al 6061-T6 under shear dominant loading," Int. J. of Fracture, 180(1), pp. 23-39.

[12] Haltom, S.S., Kyriakides, S., and Ravi-Chandar, K., 2013, "Ductile failure under combined shear and tension," Int. J. of Solids and Structures, 50, pp. 1507–1522.

[13] Faleskog, J., and Barsoum, I., 2013, "Tension–torsion fracture experiments—Part I: Experiments and a procedure to evaluate the equivalent plastic strain," Int. J. of Solids and Structures, 50, pp. 4241–4257.

[14] El-Hajjar, R., and Haj-Ali, R., 2004, "In-Plane Shear

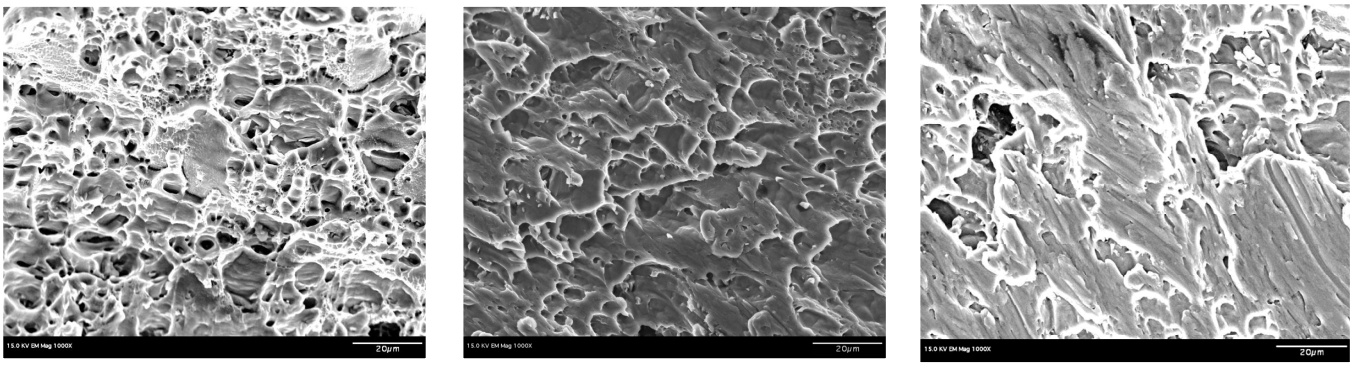

(a) tension (b) tension-torsion (c) torsion

Figure 12 SEM fractographs show failure modes.

Copyright © 20xx by ASME

Testing Of Thick-Section Pultruded FRP Composites Using A Modified Arcan Fixture," Composites: Part B, 35, pp. 421–428.

[15] Hawong J-S, Shin, D-C, and Baek, U-C, 2004, "Validation of pure shear test device using finite element method and experimental methods," Eng. Fracture Mech., 71, pp. 233–243.

[16] Jin, H., Lu, W. -Y., Foulk, J. W., III; et al., 2013, "An Examination of Anisotropic Void Evolution in Aluminum Alloy 7075," Exp Mech, 53(9), pp. 1583-1596.

Copyright © 20xx by ASME